Est. 1984

ORIENTAL JOURNAL OF CHEMISTRY
An International Open Access, Peer Reviewed Research Journal

www.orientjchem.org

ISSN: 0970-020 X
CODEN: OJCHEG
2023, Vol. 39, No.(5):
Pg. 1272-1278

Visualizing Structure Models and Patterson Densities in four WS_2 Polymorphs: Metastable (1*T'*, 4*M*) and Stable (2*H*, 3*R*) Phases

MANU KUMAR BHANDORIA[1], RAVI KUMAR RANA[1], HARI SHANKAR[2], YASHPAL SHARMA[3,1]* and JITENDRA GANGWAR[4,2]*

[1]Department of Chemistry, Baba Mastnath University, Asthal Bohar, Rohtak, Haryana, 121021, India.
[2]Indian Institute of Remote Sensing, ISRO, Dehradun, 248001, India.
[3]Department of Chemistry, RPS Degree College, Balana, Mahendergarh, Haryana, 123029, India.
[4]Department of Physics, RPS Degree College, Balana, Mahendergarh, Haryana, 123029, India.
*Corresponding author E-mail: yash.pf@gmail.com, njitendrag127@gmail.com

http://dx.doi.org/10.13005/ojc/390521

(Received: July 13, 2023; Accepted: September 30, 2023)

ABSTRACT

3-dimensional atomic and electronic structures of four crystalline WS_2 phases are rendered using VESTA program. In this study, a comprehensive investigation for visualizing structure models and Patterson densities in metastable 1*T'*- and 4M-WS_2 phases and elucidate comparison to stable 2H- and 3R-WS_2 phases. Structure models are provided in Stick, Space-filling, Ball-and-stick and Polyhedral representations with size of atoms based on their atomic radii. Analysis on type of W-S coordination (WS_6) polyhedra reveals that metastable WS_2 phases are composed of distorted octahedra and for stable WS_2 phases it is perfect trigonal prisms. Moreover, evidence of different stacking sequences in WS_2 polymorphs is also visualized. Patterson densities are exploited from model-electron and -nuclear densities are demonstrated in Wireframe representation by optimizing the interatomic distances. These studies not only evidence the structural characteristics influencing the construction of four WS_2 polymorphs, but also provide an ideal platform for both fundamental and application-oriented research.

Keywords: WS_2, Crystal Phase, Structure, Patterson densities, VESTA program.

INTRODUCTION

The fascinating phase-dependent physiochemistry of transition metal disulfides (TMDSs) in particular MS_2 (M=Ti, Zr, V, Mo, W, Fe, Re) make them as active materials for innovative applications and have enormously been investigated by many active researchers in recent years[1-12]. Among TMDSs, tungsten disulfide (WS_2; known as tungstenite in its mineral form) has been stand-out nowadays with peculiar properties such as polymorphism, optical, structural, indirect-to-direct gap transition, electro-catalytic and -chemical properties[3,7,13-17]. However, WS_2 material has attracted extensive scientific and fundamental interest because of its typical 2-dimensional (2D)

layered structure formed by covalently bonded unit S-W-S triple layers separated by weak van der Waals force[10-11,16-20]. The layered structure of WS_2 material is crucial because it entirely modifies the crystal structure and electronic properties. On the other hand, WS_2 is a ubiquitous material and is well-known to exist in a great number of different crystalline polymorphs based upon the distinct tungsten-sulfur (W-S) coordination. WS_2 usually crystallizes in monoclinic (1*T*, 1*T*', 2*M*, 4*M*), orthorhombic (T_d), hexagonal (2*H*) and rhombohedral (3*R*) type crystal structures, where first numeric and second alphabet symbols indicate the number of units in the cell and the nature of crystal system, respectively[21-27]. The 1*T*-WS_2 has octahedral (O_h) WS_6 units, 1*T*'-, T_d- and 4M-WS_2 have distorted octahedral units; whereas the perfect trigonal-prismatic (D_{3h}) coordination is obtained in 2H- and 3R-WS_2.

Among these WS_2 polymorphs, four are of tremendous attention for scientific and technological relevant applications, specifically the metastable phases 1*T*'-WS_2, 4M-WS_2 and the thermodynamically stable 2H-WS_2, 3R-WS_2 phases[28]. Additionally, the electronic configurations of WS_2 are classified into two categories according to the arrangement of S/W/S atomic planes: (i) metallic (1T'-WS_2, 4M-WS_2) and (ii) semiconducting (2H-WS_2, 3R-WS_2) phase. Owing to the most favorable phase-dependent electronic properties, WS_2 polymorphs have received much research interests for great potential in new generation technology including flat panel display, microwave absorption, energy storage, flexible nanoelectronic devices, biomedicine, lubrication, field effect transistors, superconductivity, photovoltaics, photo- and electro-catalysis applications[13,15-17,29]. Recently, several pioneering works uncovered on WS_2 polymorphs to obtain quantitative and qualitative structures, Consequently, distinctive structural features of WS_2 polymorphs are well established by a variety of theoretical and experimental investigations such as Lai *et al.,* have reported the structure characterization of phase-transformation of 1*T*'-WS_2 from 2H-WS_2[7], Song *et al.,* have discussed the detailed structural characterization of 1*T*'-WS_2 phase[21], Petkov *et al.,* have determined the 3D structure of 4M-WS_2 by atomic pair distribution function analysis[24], Zeng *et al.,* have investigated the crystal symmetry and crystallographic orientation in 2H and 3R phase WS_2[27], Lai *et al.,* have demonstrated the crystal structure characteristics of 1*T*'-WS_2 in ball-and-stick representation[28], Heijst *et al.,* have studied the atomic model of crystalline structure of 2H/3R polytype[30] and many others.

The ongoing experimental and theoretical efforts on visualizing the atomic and electronic characteristics are consistently devoted to optimize the structural features of either single or mixed WS2 polymorphs. The study on atomic structure visualization of different WS_2 polymorphs has been carried out by various methods, e.g. X-ray and/or electron diffraction, atomic resolution microscopic (HRTEM, AFM, STM) and NMR as well as Mössbauer spectroscopic techniques, comparatively a little attention has been revealed up to now the electronic/nuclear structure analysis[19,21,26,30-31]. However, no other reported studies have so far been carried out determining a comparative study on the 3D visualization of atomic structure analysis in particular unit cell parameters, atomic positions, stacking sequences and electron/nuclear densities on distinctive WS_2 phases. These features, therefore, are of utmost important for understanding the fundamental properties and outstanding practical applications of both metastable and stable WS_2 polymorphs. In order to modify, thus, the structural properties of exciting WS_2 polymorphs, by necessity, it is important to visualize the constituents in WS_2 crystal from basic physics and/or chemistry concepts viewpoint.

In the present study we have carried out a detailed investigation on the visualization of 3D structural models of WS_2 polymorphs, including metastable 1*T*'- and 4M- as well as stable 2H- and 3R-WS_2 phases. Structural representations of WS_2 polymorphs are visualized in Stick, Space-filling, Ball-and-stick and Polyhedral models based on atomic radii type. Furthermore, we demonstrated the different type of WS_6 polyhedra and layer stacking in metastable and stable WS_2 phases. Patterson densities from model electron and nuclear densities are performed in wireframe representation for visualizing the components of bond lengths in WS_2 crystal. In a nutshell, this study paves a way towards the visualization of WS_2 constituents that can be explored the phase-dependent structural properties and technologically relevant applications of this polymorphs.

Theoretical modeling

An attempt to elucidate a variety of crystallography studies in 3D visualization of WS_2 polymorphs has been made through computational method via Visuaization for Electronic STructural Analysis (VESTA) program[32]. The distinct structure models of four different WS_2 polymorphs were obtained by optimizing the structural parameters including lattice parameters, atomic parameters

and interatomic distances between metal and sulfur atoms, which then were used for an obvious visualization of WS_2 polymorphs.

RESULTS AND DISCUSSION

Structure Models

Figure 1-4 demonstrate the unit structures of distinctive WS_2 polymorphs in different structure models. The structural characteristics in terms of space group, crystal structure, type of crystal system and lattice parameters of WS_2 polymorphs are summarized in Table 1. The 3D structure models of monoclinic crystal structure with one formula unit cell of 1*T*'-WS_2 phase are visualized in Fig. 1. A stick structure model is provided in Fig. 1(a) reveals that only stick is treated as bond of tungsten (W) and sulfur (S) atoms. The space-filling structure model is presented in Fig. 1(b) demonstrating the atoms filled space in resultant unit cell. Interestingly both the W and S atoms are in distinct colour to differentiate each other. Fig. 1(c) illustrates the ball-and-stick structure model resulting the atomic size of W is larger than the S. The polyhedral structure model is established in Fig. 1(d) suggesting improved 3D visualization of structure model. The compass shows the direction of crystallography axis separately.

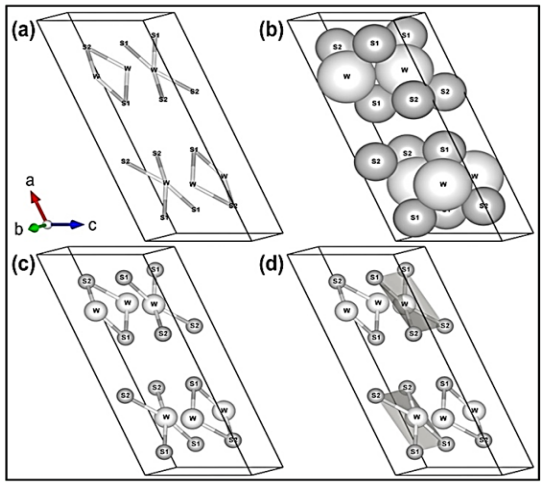

Fig. 1. Unit structures of metastable 1*T*'-WS_2 phase in (a) Stick, (b) Space-filling, (c) Ball-and-stick and (d) Polyhedral representation. Atom colors (sizes) are as follows: W, white (large); and S grey (small). The black solid lines indicate unit cell

Figure 2 displays the 3D structure models of 4*M*-WS_2 polymophs within a monoclinic unit cell containing four formula units. The structure model in stick representation is shown in Fig. 2(a) evidenced to adopt only stick as bond of W and S atoms in 4M-WS_2. Fig 2(b) reveals the space-filling structure model suggesting the W and S atoms packed the entire unit cell. The ball-and-stick representation of 4*M*-WS_2 phase is displayed in Fig. 2(c), giving out the atomic size of W atom is greater than S atom. The polyhedral structure model of this phase is represented in Fig. 2(d) indicating the W is central atom in all the polyhedral structures throughout the unit cell. The crystallography compass with axis labels is provided in Fig. 2 individually.

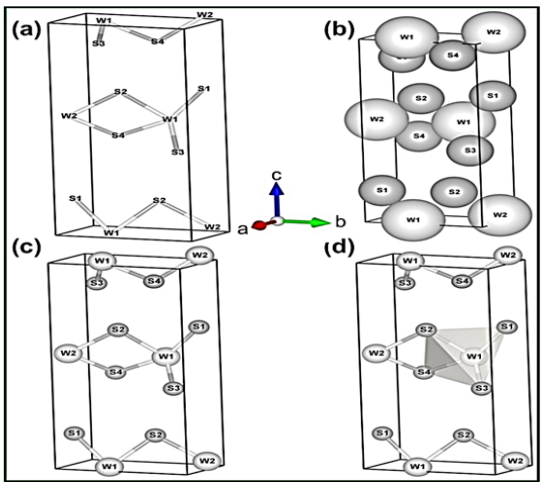

Fig. 2. Unit structures of metastable 4*M*-WS_2 phase in (a) Stick, (b) Space-filling, (c) Ball-and-stick and (d) Polyhedral representation. Atom colors (sizes) are as follows: W, white (large); and S grey (small). The black solid lines indicate unit cell

The 3D visualization of different structure models of 2*H*-WS_2 phase within a hexagonal crystal structure having two formula unit cells is evident in Fig. 3. Fig. 3(a) provides a structure model in stick representation and sticks in bicolour cylinder as bond of W and S atoms are elucidated. Fig. 3(b) exhibits the structure model in space-filling representation, the W and S atoms showed a tendency to fill the space of the corresponding hexagonal unit cell. The structure model in ball-and-stick illustration, as shown in Fig. 3(c), creates for a fascinating observation in terms of the atomic size present in the resultant unit cell. Interestingly it is found that the atomic size of W atom is bigger than the S atom, both W and S atoms are demonstrated in two different colours to distinguish each other. Fig. 3(d) illustrates the polyhedral structure model signifying the W atom is the innermost atom in all polyhedra structures. Compass with the direction of crystallography axis is shown independently in Figure 3.

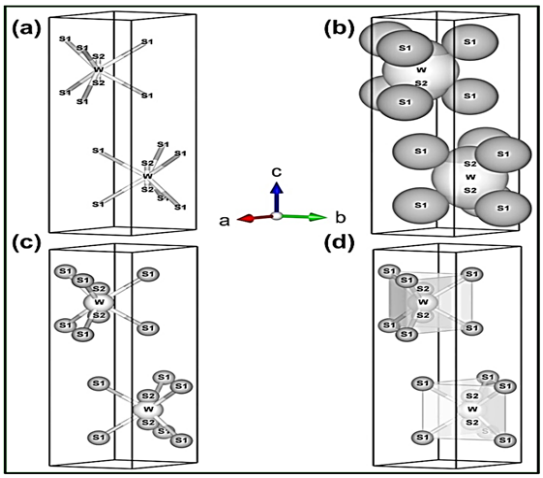

Fig. 3. Unit structures of stable 2*H*-WS_2 phase in (a) Stick, (b) Space-filling, (c) Ball-and-stick and (d) Polyhedral representation. Atom colors (sizes) are as follows: W, white (large); and S grey (small). The black solid lines indicate unit cell

Figure 4 depicts the structure models in 3D visualization of 3*R*-WS_2 polymorphs for rhombohedral crystal structure containing three formula units. Fig. 4(a) shows the structure model in stick representation demonstrating the bicolour cylinder is evidenced as the bond of W and S atoms. Space-filling structure model is visualized in Fig. 4(b) indicating the space of entire unit cell is occupied by distinct W and S atoms. Fig. 4(c) displays the structure model in ball-and-stick representation based on atomic-radii establishing the greater size of W atom than the S atom. Polyhedral representation of structure model is elucidated in Fig. 4(d) showing the W atom is the central atom in the unit cell and the W atom that can form the most bonds. The direction of crystallography axis is illustrated by a compass in Fig. 4. In Table 2 we display the atomic parameters, which are used to generate the various structure models of different WS_2 polymorphs.

WS_6 Coordination Polyhedra

The most favourable atomic-scale information on the W-S coordination is crucial to understand the thermodynamic stability of WS_2 polymorphs. Crystalline WS2 structure is built up of layers and a single-layer of WS2 can be either octahedral (WS6) or trigonal-prismatic (WS6). The upper and lower panel of Fig. 5 provide the WS6 coordination polyhedra in the ball-and-stick representation for respectively metastable 1T'- and 4M-WS2 and stable 2H- and 3R-WS2 phases. The single-layer of 1T'-WS2 is composed of distorted octahedral (WS6) in which first neighbour W-S distances are observed 2.392 and 2.451 Å for W-S1 and W-S2, respectively (as shown in Fig. 5(a)). The distortion in WS6 polyhedron of 4M-WS2 is also obtained, where the W-S distances vary as 2.434, 2.579, 2.3 and 2.469 Å for W1-S1, -S2, -S3 and -S4 and 2.534 and 2.435 Å for W2-S2 and -S4, respectively (as shown in Fig. 5(b)). While in 2H- and 3R-WS2, the single-layer is containing the perfect trigonal-prismatic (WS6) coordination and there is only a unique W-S distance of about 2.384 and 2.41 Å, respectively is exhibited (Fig. 5(c) and (d)). The variation in WS6 coordination polyhedra reveals the crystal symmetry difference between metastable phases and thermodynamically stable phases. The interatomic distances (Å) of W and S in various WS2 polymorphs are provided in Table 3.

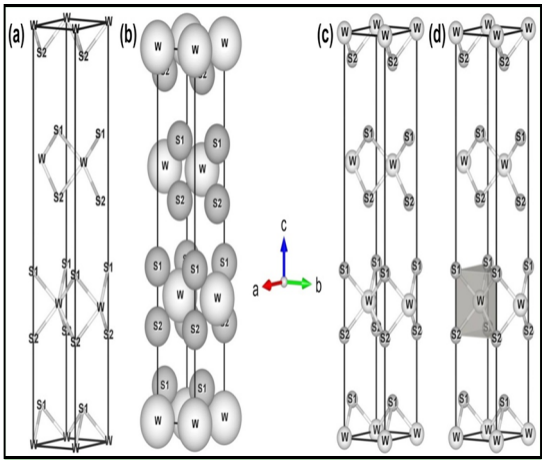

Fig. 4. Unit structures of stable 3*R*-WS_2 phase in (a) Stick, (b) Space-filling, (c) Ball-and-stick and (d) Polyhedral representation. Atom colors (sizes) are as follows: W, white (large); and S grey (small). The black solid lines indicate unit cell

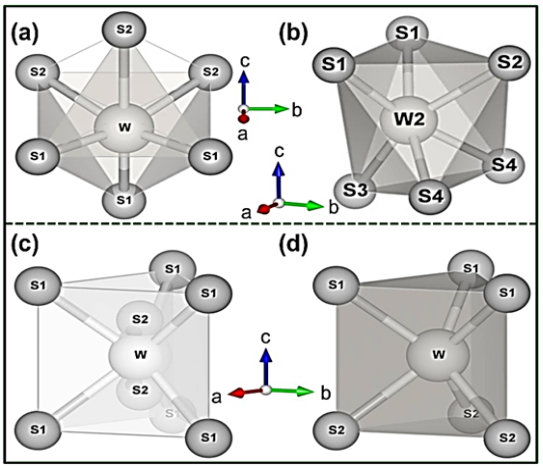

Fig. 5. Ball-and-stick with polyhedral structure models of W-S coordination type in metastable WS_2 phase (upper panel) for (a) 1*T'*-, (b) 4*M*-WS2 and stable WS_2 phase (lower panel) for (c) 2*H*-, (d) 3*R*-WS_2. Atom colors (sizes) are as follows: W, white (large); and S grey (small).

Table 1: Lattice parameters of various WS_2 polymorphs

WS_2	Space group (No.)	Crystalsystem (Lattice type)	Crystallography axis			Crystallography angle			Unit-cell volume (Å^3)
			a(Å)	b(Å)	c(Å)	α(°)	β(°)	γ(°)	
1*T'*	C2/m (12)	Monoclinic (C)	12.84	3.21	5.69	90	112.84	90	216.89
4*M*	P1121 (4)	Monoclinic (P)	3.27	5.71	12.30	90	90	88.48	230.03
2*H*	$P6_3/mmc$ (194)	Hexagonal (P)	3.15	3.15	12.32	90	90	120	106.10
3*R*	R3m (160)	Trigonal (R)	3.18	3.18	19.47	90	90	120	170.51

Table 2: Atomic parameters of W and S in various WS_2 polymorphs

WS_2 polymorphs	Atomic label	Site	Atomic positions		
			x	y	z
1*T'*-WS_2	S(1)	4i	0.104900	0	0.286500
	S(2)	4i	0.359900	0	0.179700
	W	4i	0.244200	0.500000	0.296300
4*M*-WS_2	S(1)	2a	0.082000	0.870000	0.672000
	S(2)	2a	0.546000	0.641000	0.160000
	S(3)	2a	0.542000	0.234000	-0.11300
	S(4)	2a	0.047000	0.215000	0.431000
	W(1)	2a	0.052000	0.604000	0.518000
	W(2)	2a	0.446000	-0.00200	0.040000
2*H*-WS_2	S(1)	12k	0.333000	0.667000	0.625000
	S(2)	12k	0.333000	0.667000	0.311250
	W	6h	0.333000	0.667000	0.250000
3*R*-WS_2	S(1)	3a	0.333000	0.667000	0.080779
	S(2)	3a	0	0	0.253920
	W	3a	0	0	0.000668

Table 3: Optimized interatomic distances (Å) of W and S atoms in the formation of different WS_2 polymorphs

WS_2 polymorphs	Atoms		Interatomic distances (Å)
	Atom 1	Atom 2	
1*T'*-WS_2	W	S1	2.392
	W	S2	2.451
4*M*-WS_2	W1	S1	2.434
	W1	S2	2.579
	W1	S3	2.300
	W1	S4	2.469
	W2	S2	2.534
	W2	S4	2.435
2*H*-WS_2	W	S	2.384
3*R*-WS_2	W	S	2.410

Stacking Arrangements

The stacking sequence of monolayer and multilayers in WS_2 polymorphs along z-axis is illustrated in Fig. 6. The stacking sequence is provided by a sequence of three alphabets elucidating the relative positions of S-W-S atoms in all layers. A monolayer in the 1*T'*-WS_2 phase consisting a sequence AbC Fig. 6(a). The 4*M*-WS_2 phase has stacking arrangement AbA of S atoms in the unit cell, as shown in Fig. 6(b). From Fig. 6(c), the stacking sequence AbA BaB with the S atoms overlying by the W atoms along Z-axis of the adjacent layer is obtained in 2*H*-WS_2 phase. The 3*R*-WS_2 phase has a stacking sequence AbA CaC BcB in the rhombohedral crystallographic unit cell, as shown in Figure 6(d).

Patterson Densities

The upper (lower) panel of Fig. 7 display the 3D distribution of Patterson densities from model electron (nuclear) densities in wireframe representation of WS_2 polymorphs. From Fig. 7, the wireframe structure model elucidating the visualization of charge carrier densities in only wire form and no obvious balls and sticks are evidenced. An electron density map is constructed for 1*T'*-, 4M-, 2H- and 3*R*-WS_2 phases and displayed in upper panel of Fig. 7((a), (b), (c) and (d), respectively). Green and red/orange shaded portion signifying the distribution of electron density of W and S atoms, respectively. The Patterson map indicates the strong electron density distribution at the corners of the unit cell and weak electron density is distributed in the central. In the lower panel of Fig. 7, WS_2

polymorphs display the Patterson map analysis of nuclear-densities. Owing to the strong nuclear force small shaded portions of Patterson densities from model nuclear densities are visualized

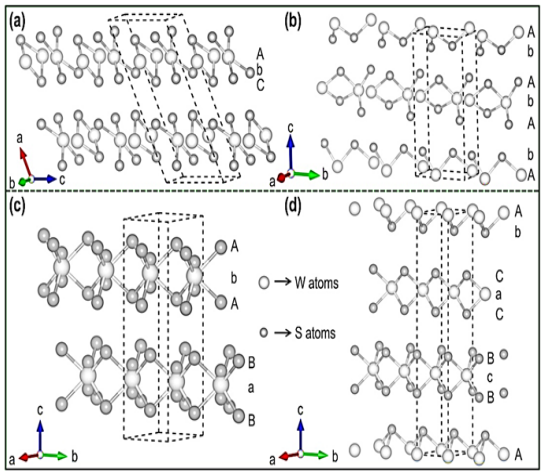

Fig. 6. Different stacking arrangements in Ball-and-stick representation of metastable WS_2 phase (upper panel) for (a) 1*T*'-, (b) 4*M*-WS_2 and stable WS_2 phase (lower panel) for (c) 2H-, (d) 3*R*-WS_2. Atom colors (sizes) are as follows: W, white (large); and S grey (small). The dashed black lines indicate the corresponding unit cell

authenticating the nucleons are confined in small region. In addition, the stable phases (2H-WS_2 and 3*R*-WS_2) have a higher density than metastable phases (1*T*'-WS_2 and 4*M*-WS_2).

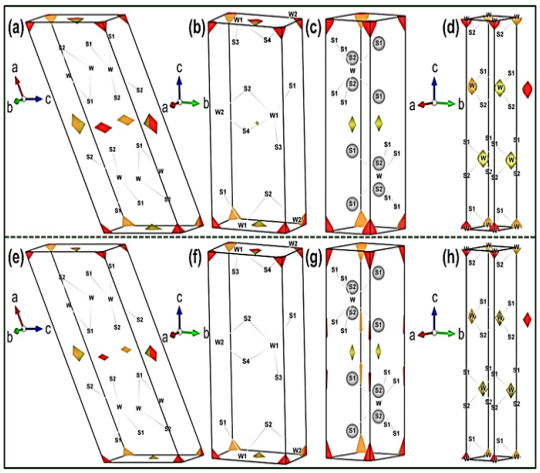

Fig. 7. Wireframe representation of Patterson densities from model electron densities (upper panel) and corresponding model nuclear densities (lower panel) for (a, e) 1*T*'-, (b, f) 4*M*-, (c, g) 2*H*-, and (d, h) 3*R*-WS_2 phases. Unit cells are outlined using solid black lines

CONCLUSION

In summary, a fascinating set of unusual structural features of WS_2 phases with emphasis on demonstrating atomic positions and bond-lengths in crystal lattices have been visualized and discussed employing VESTA program. The atomic radii-based structure models are successfully constructed in Stick, Space-filling, Ball-and-stick and Polyhedral styles for both metastable (1*T*'-, 4*M*-WS_2) and stable (2*H*-, 3*R*-WS2) phases. In addition, different WS_6 symmetry and stacking sequence in different WS_2 polymorphs are fully demonstrated. The Patterson densities are illustrated in wireframe representation by modifying the interatomic distances to elucidate the densities of constituents in WS_2 crystal phases. Overall, this robust strategy is successfully sheds light on the visualization of structural representation of WS_2 polymorphs, which is the key point of this study. This simple approach can also be utilized to understand the phase-engineering of other polymorphs materials allied to fundamental and technological interests.

ACKNOWLEDGEMENT

Support from the SERB-DST sponsored project (ECR/2017/000879; Diary No./Finance No. SERB/F/7840/2018-2019) is gratefully acknowledged.

Conflict of Interest

The authors declare no conflict of interest.

REFERENCES

1. Chia, X.; Eng, A. Y. S.; Ambrosi, A.; Tan, S. M.; Pumera, M. *Chem. Rev.*, **2015**, *115*, 11941-11966. DOI: 10.1021/acs.chemrev.5b00287
2. Sha, R.; Vishnu, N.; Badhulika, S. *IEEE Trans. Nanotechnol.*, **2022**, *21*, 374-379. DOI: 10.1109/TNANO.2022.3190223
3. Xiao, Y.; Zhou, M.; Liu, J.; Xu, J.; Fu, L. *Sci. China Mater.*, **2019**, *62*, 759-775. DOI: 10.1007/s40843-018-9398-1
4. Coriolano, A.; Polimeno, L.; Pugliese, M.; Cannavale, A. *Sci. Adv.*, **2022**, *8*, eadd8857. DOI: 10.1126/sciadv.add8857
5. Kanazawa, T.; Amemiya, T.; Upadhyaya, V.; Ishikawa, A. *IEEE Trans. Nanotechnol.*, **2022**, *16*, 582-587. DOI: 10.1109/TNANO.2017.2661403

6. Pizzochero, M.; Yazyev, O. V. *Phys. Rev. B.,* **2017**, *96*, 245402. DOI: 10.1103/PhysRevB.96.245402
7. Lai, Z.; Yao, Y.; Li, S.; Ma, L. *Adv. Mater.*, **2022**, *34*, 2201194. DOI: 10.1002/adma.202201194
8. Heising, J.; Kanatzidis, M. G. *J. Am. Chem. Soc.* **1999**, *121*, 11720-11732. DOI: 10.1021/ja991644d
9. Kim, B. H.; Kwon, S. H.; Yoon, H.; Kim, D. W.; Yoon, Y. *J. IEEE Trans. Nanotechnol.*, **2019**, *18*, 1200-1203. DOI: 10.1109/TNANO.2019.2951599
10. Güller, F.; Llois, A. M.; Goniakowski, J.; Noguera, C. *Phys. Rev. B.,* **2015**, *91*, 075407. DOI: 10.1103/PhysRevB.91.075407
11. Jha, R. K.; Guha, P. K. *IEEE Trans. Nanotechnol.*, **2018**, *17*, 582-589. DOI 10.1109/TNANO.2018.2827056
12. Kumar, N.; Borkar, H.; Siroha, P.; Kumar, R. Sens. *Actuators B: Chem.*, **2022**, *72*, 132572. DOI: 10.1016/j.snb.2022.132572
13. Mahler, B.; Hoepfner, V.; Liao, K.; Ozin, G. A. *J. Am. Chem. Soc.*, **2014**, *136*, 14121-14127. DOI: 10.1021/ja506261t
14. Zhang, S.; Guo, L.; Fan, M.; Lou, F.; Gao, P.; Lv, H.; Wang, X.; Yang, J.; Li, T.; Yang, K.; S. Zhao. *IEEE Photon. J.*, **2017**, *9*, 1-7. DOI: 10.1109/JPHOT.2017.2691740
15. Samarawickrama, P.; Dulal, R.; Fu, Z.; Erugu, U. *ACS Omega.*, **2021**, *6*, 2966-2972. DOI: 10.1021/acsomega.0c05327
16. Ratha, S.; Rout, C. S. *ACS Appl. Mater. Interfaces.*, **2013**, *5*, 11427-114. DOI: 10.1021/am403663f
17. Liu, Q.; Li, X.; Xiao, Z.; Zhou, Y. *Adv. Mater.*, **2015**, *27*, 4837-4844. DOI: 10.1002/adma.201502134
18. Zhao, C.; Che, X.; Zhang, Z.; Huang, F. *Dalton Trans.*, **2021**, *50*, 3862-3866. DOI: 10.1039/d0dt04313c
19. Xie, L.; Wang, L.; Zhao, W.; Liu, S.; Huang, W.; Zhao, Q. *Nat. Commun.*, **2021**, *12*, 5070. DOI: 10.1038/s41467-021-25381-1
20. Li, Y. W.; Zheng, H. J.; Fang, Y. Q.; Zhang, D. Q. *Nat. Commun.*, **2021**, *12*, 2874. DOI: 10.1038/s41467-021-23076-1
21. Song, X.; Singha, R.; Cheng, G.; Yeh, Y. W. *Sci. Adv.*, **2023**, *9*, eadd6167. DOI: 10.1126/sciadv.add6167
22. Fang, Y.; Pan, J.; Zhang, D.; Wang, D., *Adv. Mater.*, **2019**, *31*, 1901942. DOI: 10.1002/adma.201901942
23. Tsai, H. L.; Heising, J.; Schindler, J. L.; Kannewurf, C. R., *Chem. Mater.*, **1997**, *9*, 879-882. DOI: 10.1021/cm960579t
24. Petkov, V.; Billinge, S. J. L.; Heising, J.; Kanatzidis, M. G. *J. Am. Chem. Soc.*, **2000**, *122*, 11571-11576. DOI: 10.1021/ja002048i
25. Wang, L. S.; Fang, Y. Q.; Huang, Y. Y.; Cheng, E. *J. Phys. Rev. B.,* **2020**, *102*, 024523. DOI: 10.1103/PhysRevB.102.024523
26. Piao, M.; Yang, Z.; Liu, F. Chu, J., *J. Alloys Compd.*, **2020**, *815*, 152335. DOI: 10.1016/j.jallcom.2019.152335
27. Zeng, Z.; Sun, X.; Zhang, D.; Zheng, W., *Adv. Funct. Mater.*, **2019**, *29*, 1806874. DOI: 10.1002/adfm.201806874
28. Lai, Z.; He, Q.; Tran, T. H.; Repaka, D. V. M., *Nat. Mater.,* **2021**, *20*, 1113-1120. DOI: 10.1038/s41563-021-00971-y
29. Kim, Y. J.; Park, W.; Yang, J. H.; Kim, Y.; Lee, B. H. *IEEE J. Electron Devices Soc.*, **2018**, *6*, 164-168. DOI: 10.1109/JEDS.2017.2781250
30. Heijst, S. E. V.; Mukai, M.; Okunishi, E.; Hashiguchi, H., *Ann. Phys.*, **2021**, *533*, 2000499. DOI: 10.1002/andp.202000499
31. Stansbury, C. H.; Utama, M. I. B.; Fatuzzo, C. G.; Regan, E. C., *Sci. Adv.*, **2021**, *7*, eabf4387. DOI: 10.1126/sciadv.abf4387
32. Momma, K.; Izumi, F. *J. Appl. Cryst.*, **2011**, *44*, 1272-1276. DOI: 10.1107/S0021889811038970